

WHY BUCKLING STELLAR BARS WEAKEN IN DISK GALAXIES

Inma Martinez-Valpuesta¹ and Isaac Shlosman

Department of Physics and Astronomy, University of Kentucky, Lexington, KY 40506-0055, USA
email: martinez@pa.uky.edu, shlosman@pa.uky.edu

ABSTRACT

Young stellar bars in disk galaxies experience a vertical buckling instability which terminates their growth and thickens them, resulting in a characteristic peanut/boxy shape when viewed edge on. Using N -body simulations of galactic disks embedded in live halos, we have analyzed the bar structure throughout this instability and found that the outer (approximately) third of the bar dissolves completely while the inner part (within the vertical inner Lindblad resonance) becomes less oval. The bar acquires the frequently observed peanut/boxy-shaped isophotes. We also find that the bar buckling is responsible for a mass injection above the plane, which is subsequently trapped by specific 3-D families of periodic orbits of particular shapes explaining the observed isophotes, in line with previous work. Using a 3-D orbit analysis and surfaces of sections, we infer that the outer part of the bar is dissolved by a rapidly widening stochastic region around its corotation radius — a process related to the bar growth. This leads to a dramatic decrease in the bar size, decrease in the overall bar strength and a mild increase in its pattern speed, but is not expected to lead to a complete bar dissolution. The buckling instability appears primarily responsible for shortening the secular diffusion timescale to a dynamical one when building the boxy isophotes. The sufficiently long timescale of described evolution, ~ 1 Gyr, can affect the observed bar fraction in local universe and at higher redshifts, both through reduced bar strength and the absence of dust offset lanes in the bar.

Subject headings: galaxies: bulges — galaxies: evolution — galaxies: formation — galaxies: halos — galaxies: kinematics and dynamics — galaxies: spiral

1. Introduction

Stellar bars are among the extreme signatures of a breakup of axial symmetry in galactic disks. As such, they serve as an impetus for secular and dynamical evolution of galaxies at all redshifts. The bar formation and growth largely depend on the efficiency of angular momentum redistribution, i.e., the ability of the inner (bar unstable) disk to lose the angular momentum and of the outer disks, halos and interactions to absorb it (Athanasoula 2003). The growth of *numerical* collisionless bars can be characterized by increase in the amplitude of $m = 2$ mode and their pro-

lateness, i.e., decrease of equatorial axial ratio b/a . Bars in this initial stage of evolution appear to be as flat as the disk of their origin, with shortest-to-longest axis ratio $c/a \sim 0.1$. This is supported by numerical modeling of bar instability over nearly three decades (e.g., Sellwood & Wilkinson 1993).

Initial growth of model bars is terminated by the so-called vertical buckling instability, first detected in numerical simulations of Combes & Sanders (1981) and given two alternative explanations: a resonant bending (Combes et al. 1990; Pfenniger & Friedli 1991) and firehose instability (Raha et al. [1991], who invoked the explanation by Toomre [1966]; Merritt & Sellwood 1994). This instability leads to the vertical thickening of the bar on a dynamical timescale via spectacular

¹Also: at Department of Physics, Astronomy & Mathematics, University of Hertfordshire, Herts AL10 9AB, UK

breakup of vertical symmetry. Interest to this phenomenon has been further amplified by the similarity between frequently observed peanut- and boxy-shaped bulges in edge-on disk galaxies (e.g., Burbidge & Burbidge 1959; Jarvis 1986; Shaw 1987; Bureau & Freeman 1999; Merrifield & Kuijken 1999) and those obtained in numerical models (Patsis, Skokos & Athanassoula 2002a; Aronica et al. 2003; O’Neil & Dubinski 2003). The addition of an *inhomogeneous* dissipative component to the disk acts as to weaken the buckling and to wash out the boxy inner shape, resulting in a more ‘classical’ bulge with the shape parameter n larger by a factor of 2 (Berentzen et al. 1998).

Furthermore, numerical simulations capturing this evolution of stellar bars show them to weaken dramatically during the buckling instability. However, the reason for this drop in the bar strength was never explained. Is it caused by the buckling? Can it lead to a complete bar dissolution (e.g., Raha et al. 1991), is the bar weakened temporarily or permanently? What fraction of the orbits and which orbits stop to support the bar potential?

In this Letter we focus on the physical reasons for this behavior and provide quantitative answers to these questions. Our results are based on the self-consistent 3-D N -body simulations and a subsequent nonlinear 3-D orbit analysis of the time-dependent numerical models.

The emerging connection between the peanut/boxy bulges in edge-on disks and the buckling instability allows, in principle, to deduce the face-on properties of galaxies in their most unfavorable orientation. This instability appears to be important in understanding dynamical and secular evolution of barred galaxies. It bears direct consequences for radial redistribution of their stellar and gaseous components, and can affect the distribution of star formation sites — both depend strongly on the bar strength and its pattern speed. Lastly, this is one of the processes which contribute to the growth of the pseudo-bulges (e.g., review by Kormendy & Kennicutt 2004).

The nature of the buckling instability is being slowly understood and recent progress is based on the analysis of the orbital structure of barred (Pfenniger 1984; Skokos, Patsis & Athanassoula 2002a,b) and unbarred (Patsis et al. 2002b) disks and spheroidal components (Binney & Petrou

1985; May et al. 1985), and is related to the shapes of dominant orbital families. Observationally, significance of peanut/boxy bulges follows directly from their abundance — almost half of all edge-on disks exhibit them (Lütticke, Dettmar & Pohlen 2000). The emerging picture is that of two processes: of the firehose instability leading to the buckling in the midplane of the bar and of resonant heating, trapping the particles around stable 3-D orbits which furnish the bar with the boxy-shaped bulge. The energy deposited initially in the characteristic wavelength of buckling instability subsequently cascades down to smaller wavelengths, increasing the vertical dispersion velocities within the region.

More specifically, Pfenniger & Friedli (1991) have identified 3-D orbital families,¹ which if populated will provide the bar with the specific ‘butterfly’ or peanut shape when viewed edge-on along the minor axis. These families originate at the vertically-unstable gap of plane periodic orbits, in other words, at the vertical inner Lindblad resonance (VILR) which is almost always present in the bar, at roughly $1/3 - 2/3$ of its corotation radius. In this picture, the growth of the bar is limited by formation of unstable plane orbits (Pfenniger 1984). Those diffuse across the VILR, leading to the bar thickening in the resonance region.

2. Results

We have used version FTM-4.4 of N -body code (e.g., Heller & Shlosman 1994) with $N = 6 \times 10^5$ collisionless particles, which represent the stellar disk and dark halo components. In a number of runs, the particles have been distributed initially according to Fall & Efstathiou (1980) analytical model which consists of an iteratively-relaxed halo and an exponential disk. The dynamical time is 4.7×10^7 yrs, and r and z are the radial and vertical coordinates in the disk. The initial conditions for the model described here are chosen such that the disk/halo mass ratio within 10 kpc is unity. The halo has a flat density core of 2 kpc to avoid excessive stochastic behavior associated with the central cusps (El-Zant & Shlosman 2002). The radial and vertical disk scalelengths are 2.85 kpc

¹Their projections onto the potential midplane are elongated with the bar, similarly to the main orbit family supporting the bar

and 0.5 kpc and the Toomre’s Q parameter is 1.5. Gravitational softening of 160 pc was used. For the orbital analysis, we use the updated algorithm described in Heller & Shlosman (1996). All the discussion involving 3-D orbital structure and resonances in the bar are based on this *nonlinear* formalism and differ substantially from the epicyclic (linear) approximation. The bar pattern speed, Ω_b , is calculated from the phase angle of the $m = 2$ mode. The energy and angular momentum in the system are conserved to within approximately 1% and 0.05% accuracy, respectively. Our results appear to be reasonably independent of N .

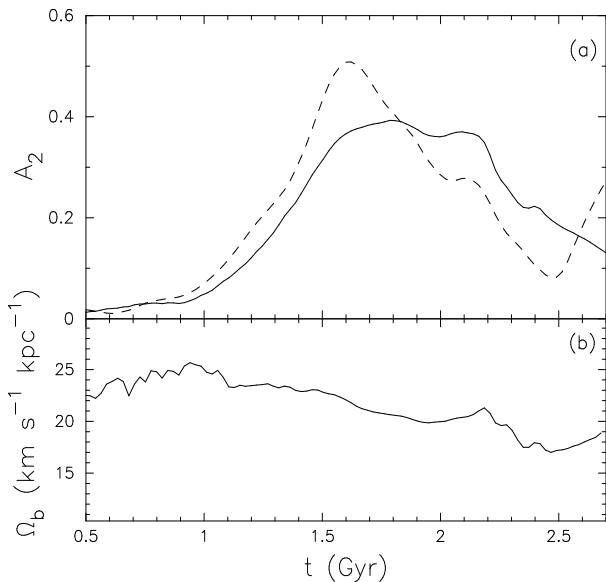


Fig. 1.— (a). Evolution of bar $m = 2$ amplitude, A_2 , for $r = 0 - 4$ kpc (solid) and $r = 6 - 10$ kpc (dashed) — inner and outer bar parts; (b). Bar pattern speed Ω_b .

The initially axisymmetric model develops a prominent bar in about three rotations (as measured by $m = 2$ amplitude A_2 , Fig. 1a), which starts to break against the halo and the outer disk, reducing its pattern speed (Fig. 1b). Between about $t \sim 1.6 - 2.4$ Gyr, the bar becomes vertically unstable and buckles, breaking the symmetry with respect to the disk equatorial midplane (Fig. 2). After $t \sim 2.4$ Gyr, the bar profile in the rz plane again tends towards symmetry, but the inner bar part has now a larger vertical thickness, $c/a \sim 0.3$, and its isophotes have acquired a boxy

appearance, in accordance with previous work on this subject. More careful analysis reveals additional fundamental changes and transformations in the bar. This subtle bar evolution can be followed through changes in its orbital structure.

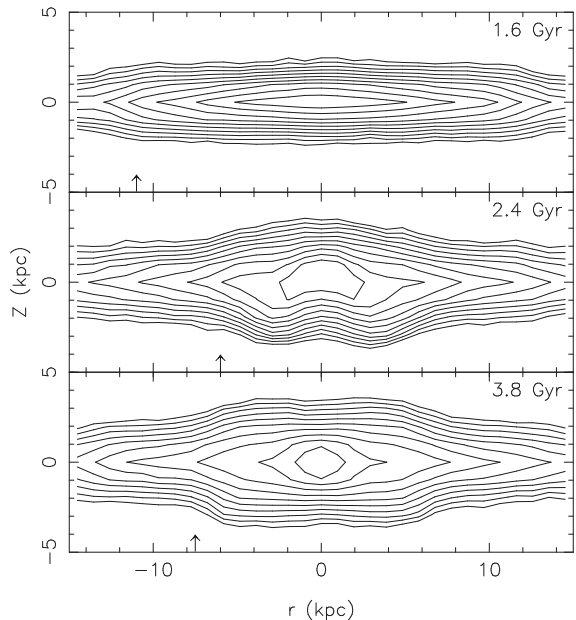


Fig. 2.— From thin bar – to buckled one – to boxy bulge: snapshots in the rz plane at $t = 1.6$ Gyr (upper), 2.4 Gyr (middle) and 3.8 Gyr (lower) given by projected isodensities, whose values have been preserved from frame to frame. The bar is oriented perpendicular to the line-of-sight. Note the dramatic shortening of inner contours. The vertical arrows indicate the approximate extent of the bar.

First, the bar size and strength change in a particular way during the short period of buckling. The size of the bar is defined here in the observational context (following Knapen, Shlosman & Peletier 2000). Namely, the bar is “detected” by the maximal ellipticity of the face-on fitted bar isophotes (i.e., isodensities), and their constant position angle (PA). Its size is taken to be the maximal radius of $\text{PA} = \text{const.}$ ² We have verified *a posteriori* that this definition does not contradict the bar size obtained from the extent of the largest

²Note, that A_2 maximum is *not* a good measure of the bar size as higher harmonics, $m = 4$ and 8, have a substantial contribution

stable periodic orbit supporting the bar figure.

The isodensity ellipse fitting to the bar at $t = 1.6$ Gyr resulted in rising ellipticity along the bar, from ~ 0.45 at the innermost to about 0.78 at $r \sim 8 - 9$ kpc and its subsequent drop. For $t = 2.4$ Gyr, the bar ellipticity stayed flat, ~ 0.5 , up to $r \sim 5$ kpc and dropped sharply for larger r . The inner part of young numerical bars hence appears by far more non-axisymmetric than in their observational counterparts.

Prior to buckling, the bar grows and extends to nearly its corotation radius, r_{CR} , which increases with time due to the decreasing Ω_{b} . Between $t \sim 1.9 - 2.4$ Gyr, the bar decreases in its length r_{b} by $\sim 1/3$, but resumes its growth afterwards. The ratio $r_{\text{CR}}/r_{\text{b}}$ is about 1.05 between $t \sim 1.4 - 1.9$ Gyr, increases to 1.7 at $t \sim 2.4$ Gyr and drops to 1.4 thereafter. At $t \sim 2.4$ Gyr, the bar size appears to correspond to $r_{\text{VILR}} \sim 0.5 - 0.6r_{\text{CR}}$, or in other words, to the radius of an unstable gap in the main family of xy planar orbits supporting the bar.

Second, as Fig. 1a reveals, the weakening of the bar starts in the outer part and propagates inwards, and while the amplitude of the inner part drops by a factor of $\sim 3 - 4$, the outer bar basically *dissolves* and its A_2 amplitude tends to zero, before it *rebounds* and grows again.

Third, the mass within the central $r \sim 1$ kpc jumps almost by a factor of 2 between $t = 1.6 - 3.8$ Gyr, and by about 20% within $r = 3$ kpc, leading to a much more centrally concentrated system. This mass concentration grows rather ‘impulsively,’ and can in principle be responsible for periods of a mild spinup in Ω_{b} seen in Fig. 1b at $t \sim 2 - 2.2$ Gyr and after 2.4 Gyr. The buckling instability also injects a (relatively) substantial disk mass above its midplane of $z = \pm 1$ kpc for $r \lesssim r_{\text{VILR}}$, increasing the mass there by a factor of ~ 6 , at $t \sim 2.4$ Gyr. We have verified that particles which are injected above the plane are those trapped by the bar prior and during the instability. Their specific angular momentum is lower than for particles remaining in the plane by about 20%. Lastly, the ratio $(\sigma_z/\sigma_r)^2$, of vertical-to-radial velocity dispersions in the bar, drops during the bar growth to just below 0.4 and then abruptly rises to about 0.95 at $t \sim 2.4$ Gyr.

3. Discussion

The bar overall weakening and dissolution of the outer part during the buckling instability are reflected in kinematical properties and changes of its orbital structure. Those are discussed without invoking a specialized terminology.

The main kinematic change during the instability is that the bar which is a very fast rotator initially, becomes a slow rotator between $\sim 2.1 - 3.3$ Gyr, and again a fast one afterwards. The definition ‘fast/slow’ is used here in the sense of the relative extent of the bar with respect to its corotation (section 2). Because the characteristic offset dust lanes delineating shocks exist only in a narrow range of a fast bar parameters (e.g., Athanassoula 1992), we do not expect them to exist or, at least, to have their usual shape, during ~ 1 Gyr of the buckling and some time thereafter, when the bar is a slow rotator. In addition, the overall weakening of the bar, which resembles more of an oval distortion during a prolonged period of time, can affect the observed bar fraction, especially at higher redshifts. This and subsequent bar growth are discussed elsewhere (Martinez-Valpuesta et al., in preparation).

We have searched for main families of planar, $z = 0$, and 3-D orbits which support the bar shape before and after the buckling. Within the bar figure the particles are largely trapped around prograde regular orbits which are aligned with the bar. The bar has a narrow vertical extent prior to the buckling and the particles, therefore, are largely confined to the bar midplane with two degrees of freedom. In agreement with other studies, we find the 3-D prograde families of orbits originating at the VILR and a retrograde family originating from 1:1 resonance — initially populated only very close to the bar xy symmetry plane. During the buckling of the bar midplane, the main planar orbits acquire the bent shape within $\sim r_{\text{VILR}}$. The particles injected above the plane (see section 2) are subsequently trapped on specific 3-D orbits (see section 1), whose x and z extensions increase sharply with their energy. Populating them will provide the bar with the peanut shape when viewed along its minor axis. The boxy shape appears somewhat later (Fig. 2, lower panel), which has been also indicated by Raha et al. (1991) for barred and by Patsis et

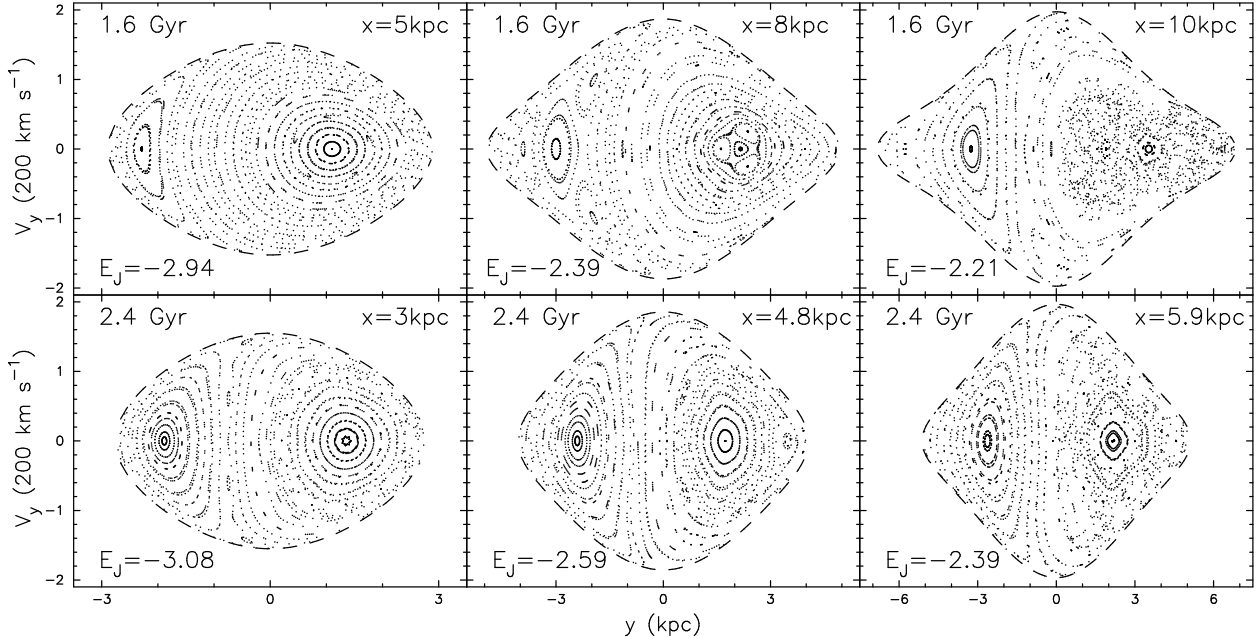


Fig. 3.— Surface of section diagrams in the (y, v_y) plane showing stochastic orbit-dominated strong bar replaced by a shorter milder bar with a larger fraction of regular orbits in the bar’s midplane, $z = 0$. This evolution happens concurrently with the buckling instability. Regular orbits form closed curves surrounding the fixed points of parent orbits. Here x and y are oriented along the major and minor axes of the bar. In the figure, $y < 0$ side represents retrograde orbits, $y > 0$ – prograde ones. Jacobi energy cuts, E_J , corresponding to r_b (right column), $0.8r_b$ (mid-column) and $0.5r_b$ (left column) have been made at two different times, $t = 1.6$ Gyr (upper frames) and $t = 2.4$ Gyr (lower frames), when the bar size drops from ~ 10 kpc to below 6 kpc. Direct and retrograde orbits dominate the phase space deeper inside the bar (distances to the center are given in the right upper corners). Note two effects: (i) much smaller fraction of the phase space occupied by regular orbits in the outer stronger bar (upper right frame) compared to dissolved outer and overall weakened bar (lower right frame); and (ii) the stochastic region expands inwards from the corotation region of the bar, dissolving its outer part, outside $x \sim 5.9$ kpc.

al. (2002b) for nearly axisymmetric disks.

An important observation by Friedli & Pfenniger (1990) that the peanut/boxy shapes appear even when the firehose instability in the bar is artificially suppressed by enforcing the symmetry in the rz plane provides the crucial insight into the role of this instability. The long evolutionary timescale of the symmetrized bar is the result of the particle diffusion process enhanced by the resonant heating via the VILR — a secular process which ultimately will furnish the bar with its characteristic peanut-shaped bulge, unless some other more efficient heating of the stellar ‘fluid’ will wash this out, e.g., star scattering by inhomogeneous gas (Berentzen et al. 1998).

How does bar buckling change this picture? The important point here appears to be particle injection above the disk plane (section 2) — those populate the characteristic 3-D family of orbits on a dynamical timescale, not secularly. Thus, the buckling accelerates the process by breaking the symmetry and by taking the evolution from the 2nd-order diffusion process to the 1st-order dynamical instability.

What exactly is responsible for the sharp drop in bar’s strength and size? The orbital structure of the bar does not itself provide the answer, as it does not supply us directly with the ‘population census’ of different orbit families. However, some measure of this, especially the fraction of phase space occupied by regular orbits, is given by

the surfaces of sections (e.g., Binney & Tremaine 1987). The bar strength is growing steadily prior to instability, and its ellipticity in the outer part is high and peaked at ~ 0.8 . Strong bars are known to generate chaos, starting from near the corotation, and the stochastic region is expected to widen with the bar strength (e.g., Contopoulos 1981). To test this, the representative surfaces of sections corresponding to regions deep inside the bar, at intermediate radii and at the bar ends are shown in Fig. 3. At $t = 1.6$ Gyr, the bar interior is dominated by a trapped regular orbits, prograde for $y > 0$ (the left two frames). The outer bar is dominated by stochastic orbits and the invariant curves have dissolved here (upper right frame). At $t = 2.4$ Gyr, however, while the stochastic region is still visible around the end of the bar, at $x = 5.9$ kpc, its fraction has decreased substantially — in tandem with the decreased bar strength. Note, that while the bar corotation propagates outwards, the stochastic region expands inwards into the bar, dissolving its part outside the peanut shape which is built at the VILR, and weakening the bar further inside. The phase space regularity is largely restored after the potential is mostly symmetrized again in the rz plane. Escaping chaotic orbits from the dissolving region have axial ratios by far different from what is needed to support the bar and rapidly precess out of the ‘valley’ of the bar potential — triggering a runaway dynamical process, concurrent with the buckling instability. Fig. 4 shows one of the highest energy stable main planar orbits in the bar at $t = 1.6$ Gyr and, for the comparison, the similar energy orbit after the buckling — much shorter in its x extension, less oval and confined to within r_{VILR} . This demonstrates the dominant trend in the bar evolution during the instability. It also underscores that the outer bar dissolution is concurrent with the buckling and maybe affected by it. The bar cannot dissolve completely as this process is clearly limited to $r \gtrsim r_{\text{VILR}}$.

In summary, a young stellar bar weakens overall and its outer part beyond the VILR dissolves after the bar reaches its peak strength. We show that this happens due to the inward expansion of the stochastic region near corotation. This effect is triggered by an exceptional strength of the growing bar prior to buckling instability. The rapidly developing chaos leads to a self-destruction of the

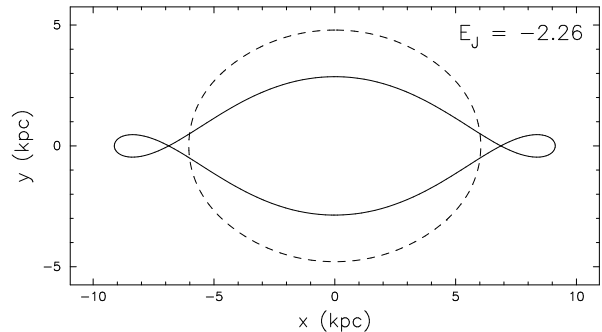


Fig. 4.— Evolution of the main family of periodic orbits supporting the bar figure at the same Jacobi energy, $E_J = -2.26$, corresponding to a long axis of $x \sim 9$ kpc at $t = 1.6$ Gyr (solid) and $x \sim 6$ kpc at $t = 2.4$ Gyr (dashed).

outer bar. There is no indication that the inner part of the bar within the VILR can dissolve. The corollary is that the bar becomes a slow rotator for about ~ 1 Gyr, a prolonged period of time, with observational consequences for gas dynamics within the bar and the formation of characteristic dust lanes there. The sharp decrease in the bar strength for a similar period of time can have implications for the observed bar fractions in local and higher redshift Universe, when both spontaneous and tidally-induced bars are important.

We are indebted to Ingo Berentzen, Amr El-Zant, Clayton Heller and Barbara Pichardo for fruitful discussions and comments on the manuscript. I.S. is supported by NASA grants NAG 5-10823 and 5-13063 and NSF AST-0206251. Additional partial support was provided by NASA through AR-09546 and 10284, from STScI which is operated the AURA, Inc., under NASA contract NAS5-26555. I.M. acknowledges partial support from PPARC. Simulations and orbital analysis have been performed on a dedicated Linux cluster and we thank Brian Doyle for technical support.

REFERENCES

- Aronica, G., et al. 2003, *ApJSS*, 284, 753
 Athanassoula, E. 1992, *MNRAS*, 259, 345
 Athanassoula, E. 2003, *MNRAS*, 341, 1179

- Berentzen, I., Heller, C.H., Shlosman, I., Fricke, K. 1998, MNRAS, 300, 49
- Binney, J., Petrou, M. 1985, MNRAS, 214, 449
- Binney, J., Tremaine, S. 1987, Galactic Dynamics, Princeton Univ. Press
- Burbidge, E.M., Burbidge, G.R. 1959, ApJ, 130, 20
- Bureau, M., Freeman, K.C. 1999, ApJ, 118, 126
- Combes, F., Sanders, R.H. 1981, A&A, 96, 164
- Combes, F., Debbasch, F., Friedli, D., Pfenniger, D. 1990, A&A, 233, 82
- Contopoulos, G. 1981, A&A 102, 265
- El-Zant, A., Shlosman, I. 2002, ApJ, 577, 626
- Fall, S.M., Efstathiou, G. 1980, MNRAS, 193, 189
- Friedli, D., Pfenniger, D. 1990, ESO/CTIO Workshop on Bulges of Galaxies, eds., B. Jarvis & D.M. Terndrup, p. 265
- Heller, C.H., Shlosman, I. 1994, ApJ, 424, 84
- Heller, C.H., Shlosman, I. 1996, ApJ, 471, 143
- Jarvis, B.J. 1986, AJ, 91, 65
- Knapen, J.H., Shlosman, I., Peletier, R.F. 2000, ApJ, 529, L93
- Kormendy, J., Kennicutt, R.C.Jr. 2004, ARA&A, in press (astro-ph/0407343)
- Lütticke, R., Dettmar, R.-J., Pohlen, M. 2000, A&AS, 145, 405
- Merrifield, M.R., Kuijken, K. 1999, A&A, 345, L45
- May, A., van Albada, T.S., Norman, C.A. 1985, MNRAS, 214, 131
- Merritt, D., Sellwood, J.A. 1994, ApJ, 425, 551
- O'Neil, J.K., Dubinski, J. 2003, MNRAS, 346, 251
- Patsis, P.A., Skokos, Ch., Athanassoula, E. 2002a, MNRAS, 337, 578
- Patsis, P.A., Athanassoula, E., Grosbol, P., Skokos, Ch. 2002b, MNRAS, 335, 1049
- Pfenniger, D. 1984, A&A, 134, 373
- Pfenniger, D., Friedli, D. 1991, A&A, 252, 75
- Raha, N., Sellwood, J.A., James, R.A., Kahn, F.D. 1991, Nature, 352, 411
- Sellwood, J.A., Wilkinson, A. 1993, Rep. Prog. Phys., 56, 173
- Shaw, M.A. 1987, MNRAS, 229, 691
- Skokos, Ch., Patsis, P.A., Athanassoula, E. 2002a, MNRAS, 333, 847
- Skokos, Ch., Patsis, P.A., Athanassoula, E. 2002b, MNRAS, 333, 861
- Toomre, A. 1966, Geophysical Fluid Dynamics, Notes on Summer Study Prog. Woods Hole Oceanographic Institution, No. 66-46, 111